Optics Letters

# Localized excitation of polarized light emission by cathodoluminescence spectroscopy

Yuhui Hu,[1] Fei Chen,[1] Yajun Gao,[1] Xiang Xiong,[1] Ruwen Peng,[1,2] and Mu Wang[1,3]

[1]National Laboratory of Solid State Microstructures, School of Physics, and Collaborative Innovation Center of Advanced Microstructures, Nanjing University, Nanjing 210093, China
[2]e-mail: rwpeng@nju.edu.cn
[3]e-mail: muwang@nju.edu.cn

Received 8 November 2017; revised 20 November 2017; accepted 21 November 2017; posted 29 November 2017 (Doc. ID 312974); published 22 December 2017

**Surface plasmons (SPs), the resonance of free electrons on the metal-air interface, may strongly interact with light and generate some extraordinary optical effects. Instead of using conventional planar light excitation, here we excite SPs with a focused electron beam on metallic nanostructures with different geometrical symmetries. With the help of a polarizer and filter in the detection system, we obtain cathodoluminescence (CL) images with different polarizations at certain wavelengths. The maxima in the CL images show that the focused electron beam may efficiently excite luminescence with different polarizations at different spots. Comparing the data collected on the structures with specific geometrical symmetry, we demonstrate that the polarization of the emitted light depends on both the structural symmetry and the excitation location. We suggest that this Letter is enlightening to understand the relationship between the SP resonance on the structure and the emission of CL with different polarizations.** 

***OCIS codes:*** (240.6680) Surface plasmons; (240.2130) Ellipsometry and polarimetry; (260.5430) Polarization.

https://doi.org/10.1364/OL.43.000158

Control of the polarization of light in a confined space is an important issue for integrated optics. It has been well established that upon illumination of light, surface plasmon (SP) resonance occurs on the metallic surface [1,2]. The surrounding electromagnetic field of the metallic structure is modulated by the irradiation of the SP resonance. At the resonant frequency, this effect is so strong that a microstructured metallic surface can effectively tune the state of light [3–9]. In recent decades, many efforts have been devoted to fully steer light and accomplish unparalleled control of anomalous reflection and refraction [10–13]. In this way, different optical devices can be achieved by engineering phase discontinuity on the interface, such as optical vortex plates [4,10] and wave plates [14]. Traditionally the SP is excited by a planar wave, which illuminates a sample surface homogeneously [15–18]. For the polarized planar wave excitation, the modes of surface charge density are anti-symmetrical along the polarization direction and symmetrical in the direction perpendicular to the polarization. Thus, the modes that are symmetrical along the polarization direction cannot be excited by the planar wave [19–23]. Moreover, for planar wave excitation, the whole sample surface is homogeneously excited, and the spectrum is collected over the whole surface. In other words, there is no spatial-resolved information in the spectrum.

In comparison, pointwise excitation with a focused electron beam possesses unique advantages. The electron beam can be focused point-by-point on the structure surface, so the spatial distribution of the luminescence capability can be measured [24,25]. The electron beam excitation occurs on a localized spot; when the spot is not coincident with the geometrical symmetry center, a symmetry-breaking effect will be observed. For example, in the scenario of planar-wave excitation on the cross-shaped structure, a symmetry-breaking effect is not expected [26]. However, with focused electron beam excitation, the situation is quite different. In addition, the wavelength of the *de Broglie* wave of electrons is much smaller than that of electromagnetic waves, so a focused electron beam excitation approach can achieve a much higher spatial resolution [27–29].

In this Letter, with cathodoluminesence (CL) spectroscopy, we investigate the polarization of light generated by a focused electron beam on the metallic structures with cross-shapes, I-shapes, and L-shapes, respectively. With a polarizer and an optical filter, we obtain CL images with specific polarization at certain wavelengths. The CL images possess different intensity distributions. Those maxima in the CL images suggest that by focusing electron beam on these spots, the luminescence with certain polarization can be most efficiently excited on the structure.

Before doing experiments, we first apply finite-difference time-domain simulations on the optical response of cross-shaped, I-shaped, and L-shaped structures. Figure 1(a) shows the scenario in which an electron beam is focused on the center of the cross (green spot); meanwhile, the whole system is quartic symmetric. When the electron beam shifts to the end of an arm of the cross (red spot), however, the quartic symmetry is broken with respect to the location of electron beam

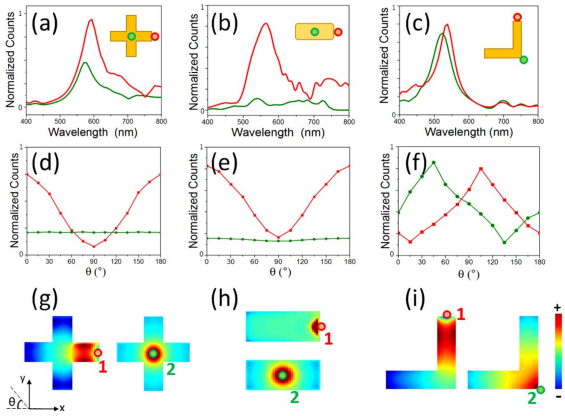


**Fig. 1.** (a)–(c) Simulated CL spectra on the cross-shaped, I-shaped, and L-shaped metallic nanostructures, respectively. (d)–(f) show the simulated intensity of the emitted luminescence with an electron beam focusing at the spots shown in (a)–(c). $\theta$ stands for the polarization direction with respect to the $x$-axis in the $x$–$y$ plane. (g)–(i) show the $z$ component of the electric field on the cross-shaped structure at 600 nm, on the $I$-shaped structure at 550 nm, and on the $L$-shaped structure at 530 nm.

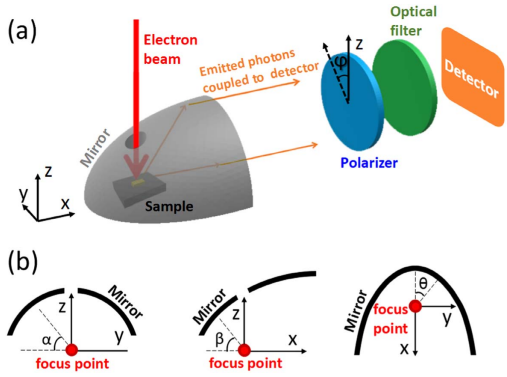


**Fig. 2.** (a) Schematics of a CL system. An electron beam incidents normal to the sample as a local excitation source, and the luminescence emits due to the SP resonance. The luminescence is collected by the reflection of a parabolic mirror. A polarizer and an optical filter are applied. (b) Schematics to show $yz$-, $xz$-, and $xy$-section plan of the parabolic mirror.

incidence. By truncating the arms of the cross pattern, we can get I-shaped [Fig. 1(b)] and L-shaped [Fig. 1(c)] structures, where the quartic symmetry disappears accordingly. Figures 1(d)–1(f) are the simulated intensities of luminescence collected at different rotation angles of the polarizer, which are excited on the cross-shaped, I-shaped, and L-shaped structures, respectively. Figure 1(d) indicates that when the electron beam is focused at the red point of the cross, the emitted light is polarized and has the highest intensity at $\theta = 0°$ and $\theta = 180°$. When the electron beam moves to the green point (the geometrical center of the structure), the emitted light is no longer polarized. Figure 1(e) shows that when the structure is excited at the red point of the $I$-shaped structure, the emitted light is polarized and has the highest intensity at $\theta = 0°$ and $\theta = 180°$ as well. However, when the electron beam shifts to the green point, the whole system is two-fold symmetric, and the emitted light is no longer polarized. Figure 1(f) indicates that when the electron beam focuses at the red and the green points on the L-shaped structure, the emitted lights are both polarized and have peak intensities at $\theta = 105°$ and $\theta = 45°$, respectively.

Further, we simulate the distribution of the z-component electric field ($E_z$), which is expected to be proportional to the distribution of surface charge density [23]. Figure 1(g) illustrates $E_z$ on the cross-shaped structure at 600 nm. When the electron beam focuses at the end of an arm, the quartic symmetry vanishes in $E_z$. However, when the electron beam is on the structural center, the field distribution is quartic symmetric. For the $I$-shaped structure, the field distribution is illustrated in Fig. 1(h). When the electron beam focuses at one end of the structure, the field distribution is asymmetric. When the electron beam focuses at the center, the field distribution becomes two-fold symmetric. For the $L$-shaped structure (the truncated cross pattern), when the electron beam focuses at the red and the green spots in Fig. 1(i), $E_z$ does not preserve any quartic symmetry at all.

The resonance on each arm of the cross-shaped structure can be treated as connected dipoles. The radiation theory of dipoles [30–32] indicates that the polarization of the emitted light depends on the symmetry of the structure. If the resonance mode is rotationally symmetric, its emission will not be polarized. However, when two or three arms of the cross pattern have been truncated, previous symmetry is broken; then the emission is polarized. This means that the polarization of the emission is determined not only by structural symmetry, but also by the location of excitation.

Our CL experiments are set as follows. A 10 KeV electron beam is focused on the structure as a local excitation source, and the luminescence emitted from the structure due to the SP resonance is collected by a parabolic mirror and is directed to a polarizer and an optical filter before reaching the photomultiplier tube detector, as illustrated in Fig. 2(a). By rotating angle $\varphi$ of the polarizer, one may determine the polarization of luminescence light at certain wavelengths [Fig. 2(a)].

It should be pointed out that when the emitted light is reflected by the parabolic mirror, its polarization state is changed. According to Yamamoto *et al.* [33], the reflected polarized light by a metallic mirror can be denoted as $s$- and $p$-polarized lights. As an approximation, the reflectivity of $s$- and $p$-polarized light can be taken as 1 in a wide-angle range [34]. It follows that a $y$-polarized light ($E_y$) reflected by the parabolic mirror is directed in the $x$-direction, as shown in Fig. 2(b). The reflected light can be written as $y$-polarized $E_{y\text{-}y}$ and $z$-polarized $E_{y\text{-}z}$, and their intensities can be expressed as surface integrals as [33,34]

$$E_{y\text{-}y} = \oiint E_y \sin^2\alpha \mathrm{d}\alpha\mathrm{d}\beta,$$
$$E_{y\text{-}z} = \oiint E_y \sin\alpha\cos\alpha \mathrm{d}\alpha\mathrm{d}\beta. \quad (1)$$

Similarly, for an $x$-polarized light ($E_x$) reflected by the parabolic mirror, the $E_{x\text{-}y}$ and $E_{x\text{-}z}$ can be respectively expressed as

$$E_{x\text{-}y} = \oiint E_x \cos\alpha \sin\beta \mathrm{d}\alpha\mathrm{d}\beta,$$
$$E_{x\text{-}z} = \oiint E_x \sin\alpha \sin\beta \mathrm{d}\alpha\mathrm{d}\beta. \quad (2)$$

The surface integrals in Eqs. (1) and (2) lead to $E_{y\text{-}y} > E_{y\text{-}z}$ and $E_{x\text{-}y} < E_{x\text{-}z}$. This means that the $x$-polarized light reflected by the mirror changes to a partially $z$-polarized light, while the $y$-polarized light reflected by the mirror changes to a partially

$y$-polarized light. Note that the partially polarized light can be decomposed to polarized light and natural light. Therefore, when we measure the CL image, if the maxima are observed with the polarizer being set in the $y$-direction and cannot be observed with the polarizer being set in the $z$-direction, this means that the electron beam excites $y$-polarized light at the maxima regions more efficiently. If these maxima appear with the polarizer set in the $z$-direction and vanish with the polarizer set in the $y$-direction, this suggests that the electron beam excites $x$-polarized light at the maxima more efficiently.

Based on this understanding, we measure CL images with the polarizer set as $\varphi = 0°$ and $\varphi = 90°$. The optical filter ensures that we collect a CL image at a certain wavelength, and the bandwidth is 50 nm. This bandwidth makes it possible to accommodate the shifted resonant wavelengths when the electron beam is focused at different spots on the structure [as that shown in Figs. 1(a) and 1(c), for example]. Experimentally, we fabricate gold $I$-shaped, $L$-shaped, and cross-shaped structures on the silicon substrate by electron beam lithography, followed by lift-off processing. The thickness of the gold layer is 50 nm, and a 2 nm thick adhesion layer of titanium is deposited on a silicon surface before gold deposition. At each excitation spot, we collect the spectrum in the range of 300–900 nm, and the integration time is set as 4.0 s. To get CL spectral images, the electron beam scans the whole structure surface pixel by pixel and, for each excitation spot, the luminescence intensity over the whole structure is collected. Therefore, the intensity distribution on such a CL image reflects the capability of local luminescence emission induced by the focused electron beam. The experimental results are shown in Figs. 3–5.

Figure 3 shows the experimental results on the cross-shaped structure. The spectra are measured with an electron beam focused at the red and green spots [Fig. 3(a)]. The SEM micrograph of the structure is illustrated in Fig. 3(b). The length of each arm of the cross is 200 nm, and the arm width is 100 nm. In Fig. 3(c); from the measured spectra, we can find when the electron beam is focused at the cross center and at the end of an arm that both of the CL spectra have peaks around 600 nm. The peak measured at the green spot is slightly blueshifted with respect to that measured at the red spot. The overall CL intensity by exciting at the end of an arm is higher than that exciting at the cross center. The CL image of the structure is collected at 600 nm. One may find that the maxima locate at the end of each arm. This means that at wavelength 600 nm the electron beam can excite luminescence much more efficiently at the end of each arm. With the polarizer, we can obtain CL images at different polarizations. Figure 3(e) shows the CL image with the polarizer set as $\varphi = 0°$, and Fig. 3(f) shows the CL image at $\varphi = 90°$. Comparing Figs. 3(e) and 3(f), we can find that the maxima distribute at the ends of the horizontal arms for $\varphi = 0°$, and the maxima appear at the ends of the vertical arms for $\varphi = 90°$. This suggests that the electron beam can excite $x$-polarized light more efficiently at the ends of horizontal arms, and can excite $y$-polarized light more efficiently at the ends of vertical arms. Therefore, we may select the polarization of the emission by focusing electron beam at different spots on the cross.

For comparison, we measure CL images of the $I$-shaped and the $L$-shaped structures. For the $I$-shaped structure, the spectra are measured by focusing the electron beam at the red and the green points [Fig. 4(a)]. Figure 4(b) illustrates the SEM micrograph of the gold bar, which is 300 nm long and 110 nm wide. Figure 4(c) shows the CL spectra by exciting at the red and green spots, which have the peaks around 550 nm, and the spectrum measured at the green spot has a slightly blueshifted peak. The CL image of the bar is obtained at 550 nm. Two maxima appear at the ends of the bar. By adding the polarizer, we find that the maxima appear for $\varphi = 0°$, and disappear for $\varphi = 90°$. This means that $x$-polarized light can be efficiently excited by focusing an electron beam at the ends of the bar.

Figure 5 demonstrates the experimental data measured on an L-shaped structure, which has been rotated by 45° with respect to $x$-axis. The CL spectrum is obtained by focusing the electron beam at red and green spots, respectively [Fig. 5(a)]. The SEM micrograph of the structure is shown in Fig. 5(b). Each arm of the L-shaped structure is 270 nm long and 90 nm wide. From Fig. 5(c), one can find that the spectrum measured at the red spot has a peak around 530 nm, whereas the spectrum measured at the green spot has a slightly blueshifted peak. The CL image obtained at 530 nm is shown in Fig. 5(d), indicating that the maxima locate at the corner of the L-shaped structure and the ends of two arms. The CL

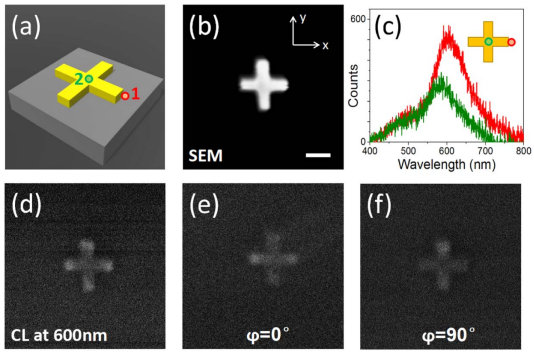


**Fig. 3.** (a) Schematics of the cross-shaped structure with two excitation spots. (b) SEM micrograph of the gold sample; the bar represents 200 nm. (c) CL spectra collected at the red spot (red curve) and the green spot (green curve) shown in (a). (d) CL image at 600 nm, measured without a polarizer. (e)–(f) CL images at 600 nm measured with a polarizer set as $\varphi = 0°$ and $\varphi = 90°$, respectively.

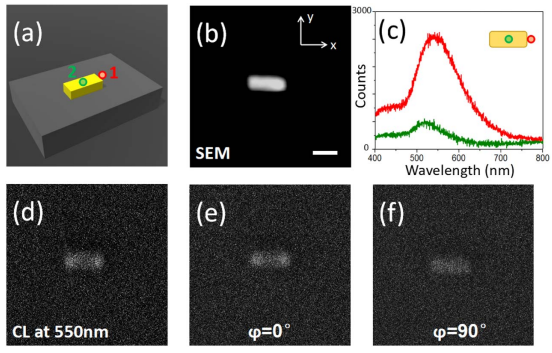


**Fig. 4.** (a) Schematics of the I-shaped structure with the excitation spot marked as red and green dots at the end of the bar. (b) SEM micrograph of the gold bar. The scale bar represents 200 nm. (c) CL spectra collected at red and green dots shown in (a). (d) CL image of the structure at 550 nm, measured without a polarizer. (e)–(f) CL images at 550 nm with a polarizer set as $\varphi = 0°$ and $\varphi = 90°$, respectively.

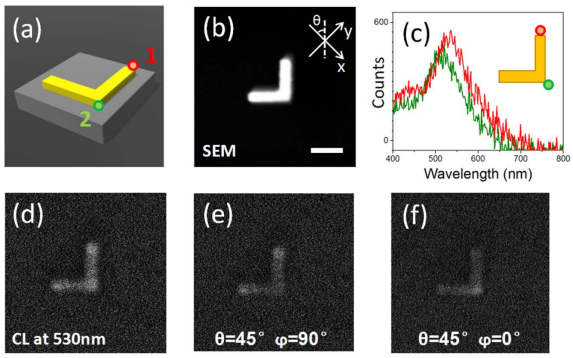


**Fig. 5.** (a) Schematics of the *L*-shaped structure, which is rotated by 45° with respect to the *x*-axis. (b) SEM micrograph of the sample. The bar represents 200 nm. (c) CL spectra obtained at the red spot (red curve) and at the green spot (green curve) shown in (a). (d) CL image of the L-shaped structure obtained at 530 nm without a polarizer. (e)–(f) CL images obtained at 530 nm with a polarizer set as $\varphi = 90°$ and $\varphi = 0°$, respectively.

images are shown in Fig. 5(e) (polarizer $\varphi = 90°$) and Fig. 5(f) (polarizer $\varphi = 0°$). For the scenario $\varphi = 90°$, maxima appear at the two ends of the arms, whereas a maximum appears at the corner of the L-shape for $\varphi = 0°$. These observations indicate that the focused electron beam can excite *y*-polarized light more efficiently at the ends of the arms, and can excite *x*-polarized light more efficiently by exciting at the corner of the *L*-shape.

Conventionally, the SP resonance on a metallic structure can be detected by near-field scanning optical microscopy. With CL spectroscopy, however, we can sense the resonance on the structure and get the relationship between the polarization of the emitted light and the geometrical symmetry of the structures. When the electron beam is focused at the center of the cross, the system is quartic symmetric, and the emitted light is nonpolarized. When the electron beam shifts to the end of each arm of the cross, the symmetry is broken, so the emitted light is polarized. Instead of exciting SPs at the asymmetric spots on the symmetric structure, we can also take the approach of decreasing the symmetry of the structure itself. By removing three or two arms of the cross, *I*-shaped or *L*-shaped structures are generated, respectively. The luminescence generated on these less symmetric structures is polarized. If we consider the resonance on each arm of the structure as a dipole, the emitted light is nonpolarized when the system is *n*-fold symmetric (here *n* is a positive integer greater than or equal to 2). Once the *n*-fold symmetry is broken, the emission then turns out to be polarized.

In conclusion, we experimentally demonstrate here that light with different polarizations can be excited by focusing an electron beam on structures with different geometrical symmetries. The polarization of the emission is determined by both the structural geometry and the excitation location. We suggest that our results help to understand microscopic mechanisms of generating polarized emission, and demonstrate a different approach to obtain luminescence light with a specific polarization.

**Funding.** National Key R&D Program of China (2017YFA0303702); National Natural Science Foundation of China (NSFC) (11474157, 11634005, 11674155, 61475070, 11574141, 11704179); "333 Project" Government of Jiangsu Province (BRA2016350).

## REFERENCES

1. H. Raether, *Surface Plasmons on Smooth and Rough Surfaces and on Gratings* (Springer, 1988).
2. W. L. Barnes, A. Dereux, and T. W. Ebbesen, Nature **424**, 824 (2003).
3. D. R. Smith, W. J. Padilla, D. C. Vier, S. C. Nemat-Nasser, and S. Schultz, Phys. Rev. Lett. **84**, 4184 (2000).
4. P. Genevet, N. Yu, F. Aieta, J. Lin, M. A. Kats, R. Blanchard, M. O. Scully, Z. Gaburro, and F. Capasso, Appl. Phys. Lett. **100**, 013101 (2012).
5. R. G. Hunsperger, *Integrated Optics: Theory and Technology* (Springer, 2009).
6. H. Wei, Z. Wang, X. Tian, M. Käll, and H. Xu, Nat. Commun. **2**, 387 (2011).
7. Y. M. Liu and X. Zhang, Chem. Soc. Rev. **40**, 2494 (2011).
8. Z. Fang and X. Zhu, Adv. Mater. **25**, 3840 (2013).
9. A. V. Kildishev, A. Boltasseva, and V. M. Shalaev, Science **339**, 1232009 (2013).
10. N. Yu, P. Genevet, M. A. Kats, F. Aieta, J.-P. Tetienne, F. Capasso, and Z. Gaburro, Science **334**, 333 (2011).
11. X. Ni, N. K. Emani, A. V. Kildishev, A. Boltasseva, and V. M. Shalaev, Science **335**, 427 (2012).
12. S. Sun, K. Y. Yang, C. M. Wang, T. K. Juan, W. T. Chen, C. Y. Liao, Q. He, S. Xiao, W. T. Kung, G. Y. Guo, L. Zhou, and D. P. Tsai, Nano Lett. **12**, 6223 (2012).
13. A. Pors, M. G. Nielsen, R. L. Eriksen, and S. I. Bozhevolnyi, Nano Lett. **13**, 829 (2013).
14. N. Yu, F. Aieta, P. Genevet, M. A. Kats, Z. Gaburro, and F. Capasso, Nano Lett. **12**, 6328 (2012).
15. M. L. Brongersma, J. W. Hartman, and H. A. Atwater, Phys. Rev. B **62**, R16356 (2000).
16. C. Dahmen, B. Schmidt, and G. von Plessen, Nano Lett. **7**, 318 (2007).
17. X. Xiong, W. H. Sun, Y. J. Bao, R. W. Peng, M. Wang, C. Sun, X. Lu, J. Shao, Z. F. Li, and N. B. Ming, Phys. Rev. B **80**, 201105 (2009).
18. S. C. Jiang, X. Xiong, Y. S. Hu, Y. H. Hu, G. B. Ma, R. W. Peng, C. Sun, and M. Wang, Phys. Rev. X **4**, 021026 (2014).
19. E. J. R. Vesseur and A. Polman, Appl. Phys. Lett. **99**, 231112 (2011).
20. F. F. Wen, J. Ye, N. Liu, P. Van Dorpe, P. Nordlander, and N. J. Halas, Nano Lett. **12**, 5020 (2012).
21. M. Frimmer, T. Coenen, and A. F. Koenderink, Phys. Rev. Lett. **108**, 077404 (2012).
22. K. H. Fung, A. Kumar, and N. X. Fang, Phys. Rev. B **89**, 045408 (2014).
23. T. Coenen, F. B. Arango, A. F. Koenderink, and A. Polman, Nat. Commun. **5**, 3250 (2014).
24. J. B. Lassiter, H. Sobhani, M. W. Knight, W. S. Mielczarek, P. Nordlander, and N. J. Halas, Nano Lett. **12**, 1058 (2012).
25. Y. H. Hu, D. Zhao, Z. H. Wang, F. Chen, X. Xiong, R. W. Peng, and M. Wang, Opt. Lett. **42**, 1744 (2017).
26. H. Wang, Y. Wu, B. Lassiter, C. L. Nehl, J. H. Hafner, P. Nordlander, and N. J. Halas, Proc. Natl. Acad. Sci. USA **103**, 10856 (2006).
27. E. J. R. Vesseur, R. Waele, M. Kuttge, and A. Polman, Nano Lett. **7**, 2843 (2007).
28. C. E. Hofmann, E. J. R. Vesseur, L. A. Sweatlock, H. J. Lezec, F. J. García de Abajo, A. Polman, and H. A. Atwater, Nano Lett. **7**, 3612 (2007).
29. P. Chaturvedi, K. H. Hsu, A. Kumar, K. H. Fung, J. C. Mabon, and N. X. Fang, ACS Nano. **3**, 2965 (2009).
30. L. Novotny, Phys. Rev. Lett. **98**, 266802 (2007).
31. G. W. Bryant, F. J. García de Abajo, and J. Aizpurua, Nano Lett. **8**, 631 (2008).
32. R. Gómez-Medina, N. Yamamoto, M. Nakano, and F. J. García de Abajo, New J. Phys. **10**, 105009 (2008).
33. N. Yamamoto, J. C. H. Spence, and D. Fathy, Philos. Mag. B **49**, 609 (1984).
34. Y. Ohno and S. Takeda, J. Electron Microsc. **51**, 281 (2002).